arXiv:1401.0484v1 [astro-ph.IM] 2 Jan 2014

Parallax Beyond a Kiloparsec from Spatially Scanning the Wide Field Camera 3 on the Hubble Space Telescope[1]

Adam G. Riess[2,3], Stefano Casertano[3,2], Jay Anderson[3], John MacKenty[3], and Alexei V. Filippenko[4]

ABSTRACT

We use a newly developed observing mode on the *Hubble Space Telescope (HST)* and Wide Field Camera 3 (WFC3), spatial scanning, to increase source sampling a thousand-fold and measure changes in source positions to a precision of 20–40 μas, more than an order of magnitude better than attainable in pointed observations. This observing mode can usefully measure the parallaxes of bright stars at distances of up to 5 kpc, a factor of ten farther than achieved thus far with *HST*. Long-period classical Cepheid variable stars in the Milky Way, nearly all of which reside beyond 1 kpc, are especially compelling targets for parallax measurements from scanning, as they may be used to anchor a determination of the Hubble constant to $\sim$ 1%. We illustrate the method by measuring to high precision the parallax of a classical Cepheid, SY Aurigae, at a distance of more than 2 kpc, using 5 epochs of spatial-scan data obtained at intervals of 6 months. Rapid spatial scans also enable photometric measurements of bright Milky Way Cepheids—which would otherwise saturate even in the shortest possible pointed observations—on the same flux scale as extragalactic Cepheids, which is a necessity for reducing a leading source of systematic error in the Hubble constant. We demonstrate this capability with photometric measurements of SY Aur on the same system used for Cepheids in Type Ia supernova host galaxies. While the technique and results presented here are preliminary, an ongoing program with *HST* is collecting such parallax measurements for another 18 Cepheids to produce a better anchor for the distance scale.

Subject headings: galaxies: distances and redshifts—cosmology: observations—cosmology: distance scale—supernovae: general

---

[1]Based on observations with the NASA/ESA *Hubble Space Telescope*, obtained at the Space Telescope Science Institute, which is operated by AURA, Inc., under NASA contract NAS 5-26555.

[2]Department of Physics and Astronomy, Johns Hopkins University, Baltimore, MD 21218.

[3]Space Telescope Science Institute, 3700 San Martin Drive, Baltimore, MD 21218; ariess@stsci.edu.

[4]Department of Astronomy, University of California, Berkeley, CA 94720-3411.

1. Introduction

The increased precision of the cosmological model in the past decade has been paralleled by a steady narrowing of the uncertainty in the Hubble constant, the parameter which sets the present age and size scale of the Universe. The first decade of the *Hubble Space Telescope (HST)* was used to refine the value of the Hubble constant (H_0) to $\sim \pm 10\%$, primarily by resolving Cepheids in distant galaxies used to calibrate a diverse set of secondary distance indicators (Freedman et al. 2001; Sandage et al. 2006). However, further progress from these distance ladders was restricted by systematic uncertainties in their rungs. Riess et al. (2011) sharply reduced the uncertainty to 3.5% through four improvements in the distance ladder comprised of Cepheids and Type Ia supernovae (SNe Ia): (1) calibrating eight modern SNe Ia with Cepheids, (2) observing Cepheids in the near-infrared (NIR) to reduce the impact of extinction and metallicity, (3) the use of two new geometric calibrations of Cepheids—parallaxes of Galactic Cepheids from the *HST* Fine Guidance Sensor (FGS; Benedict et al. 2007) and the 3% geometric maser distance to NGC 4258 (Humphreys et al. 2013, and references therein), and (4) calibrating all extragalactic Cepheid photometry with a single camera, WFC3, to negate cross-instrument zeropoint errors. This measurement agrees within 2% with three subsequent determinations of H_0 (Freedman et al. 2012; Sorce et al. 2012; Suyu et al. 2012a), and it now constrains the cosmological model with similar leverage as baryon acoustic oscillations and high-redshift SNe Ia when combined with the cosmic microwave background data (CMB; Sullivan et al. 2011).

Yet an outstanding enigma in the cosmological model remains. What is the nature of the dark energy accelerating the expansion of the Universe? A measurement of H_0 approaching percent-level precision would provide outstanding leverage for constraining the dark energy equation-of-state parameter $w = P/(\rho\ c^2)$ (Hu 2005; Suyu et al. 2012b; Weinberg et al. 2013). Using the distance ladder to reach this goal requires an improvement in the measurement of its first rung, the nearby geometric determination of distance.

Trigonometric parallaxes are the "gold standard" of local distance measurements—the simplest, the most direct, and the most assumption-free. They can be used to anchor an assortment of primary and secondary distance indicators which sample the smooth expansion of the Universe to measure the Hubble constant.

However, useful parallax measurements are among the most challenging to acquire owing to the enormous distances to most objects of interest. Only a few tens of systems have parallaxes greater than $0\farcs2$ ($D < 5\,\mathrm{pc}$). Parallax measurements from ground-based facilities have been limited by atmospheric refraction and flexure (gravitational and thermal), with the zenith of efforts reached in the *General Catalogue of Trigonometric Parallaxes* (van Altena et al. 1995), which contains parallaxes for 8,112 stars with a typical accuracy of $0\farcs01$. *Hipparcos*, a space-based facility, measured parallaxes to a mean precision of 1 mas, providing parallaxes to 10% precision or better for 20,853 stars, and to 20% or better for 49,399 stars (Perryman 2009). More recently, the Very Long Baseline Interferometer (VLBI) has been used at radio wavelengths to measure parallaxes

with $\sim 10\,\mu$as precision beyond a kiloparsec for a sample of sources distinguished by their radio brightness (primarily star-forming regions, pulsars, and masers near asymptotic giant branch stars) (Reid & Honma 2013). Unfortunately, this approach is not applicable to most kinds of stars.

Long-period Galactic Cepheids ($P > 10$ days) are among the most coveted targets for parallax measurements, but they reside beyond the capability of what has been feasible so far. Cepheids remain such vital targets because of their preeminent role as carriers of the distance scale to extragalactic objects (Leavitt & Pickering 1912). These pulsating supergiants are relatively rare; several hundred are known in the Galaxy, with distances D from the Sun ranging from 0.1 to 10 kpc. The closest, Polaris ($D = 0.13$ kpc), is less useful as a distance indicator because it pulsates in an overtone mode. The closest fundamental pulsator is the class namesake, δ Cephei, at $D = 0.27$ kpc and $P = 5.37$ days . Useful measurements beyond 0.1 kpc demand astrometric precision of better than 1 mas and repeatability over a year or more, a task made easier by the resolution and stability of a space-based observatory.

Benedict et al. (2007) used 110 *HST* orbits and the two FGSs to measure parallaxes for 9 Cepheids with $D < 0.5$ kpc with an individual precision of $\sim 8\%$, providing one of the best anchors of the measurement of the Hubble constant to date (Riess et al. 2009, 2011; Freedman et al. 2012). (The FGSs provide the most precise optical measurements of relative position, to 0.3 milliarcseconds (henceforth mas) for bright stars, a factor of 3 more precise than the *Hipparcos* observatory). However, the accuracy of H_0 determined via the FGS sample is limited by several factors: (i) its mean distance is determined to an accuracy of $\sim 3\%$; (ii) they are too bright to image on the same *HST* system used to observe extragalactic Cepheids along the distance ladder, introducing an additional 2% systematic error; (iii) their mean period ($\langle P \rangle = 6$ days) is much shorter than those of the extragalactic Cepheids visible at $D > 20$ Mpc with *HST* in SN Ia hosts ($\langle P \rangle = 30$ days), propagating a systematic uncertainty of 2% in the Hubble constant per 5% uncertainty in the slope of the P–L relation. In addition, use of a simple linear extrapolation of the Cepheid NIR P–L relation to bridge the period gap between calibration and application is risky, especially given the discovery of a break in the *optical* P–L relation at $P = 10$ days (Ngeow et al. 2005).

Unfortunately, all long-period Milky Way (MW) Cepheids, except one, are at $D > 1$ kpc. Conventional imaging limits the astrometric precision of an unresolved, bright target to 0.01 pixel for WFC3-UVIS or $400\,\mu$as (Bellini et al. 2011), no better than a 2σ detection of parallax at 2 kpc. To realize a 1% calibration of the Hubble constant, we need to calibrate a new sample of Galactic Cepheids whose periods *bracket* those in extragalactic samples, while also obtaining their photometry on the same *HST* system used for extragalactic Cepheids. Thus, we need to extend the range of *HST*-based parallaxes to $D > 1$ kpc. While the GAIA mission is expected to obtain 10–20 μas parallaxes across the sky by the mission's end, the extreme brightness of long-period MW Cepheids compromises its ability to accurately measure many of these targets which have $V < 7$ mag; moreover, even with successful parallax measurements from GAIA, the need for homogeneous photometry of MW and extragalactic Cepheids will remain.

In pursuit of these goals, we have developed a new method for obtaining useful measurements of stellar parallaxes with *HST* at greater distances than previously possible. *Spatial scans*, recently implemented on *HST* for WFC3-UVIS to measure exoplanet transits (McCullough & MacKenty 2012), can be used to sample (i.e., reobserve) the target and astrometric reference stars in the field thousands of times to provide an enormous boost in astrometric precision over pointed imaging. By scanning perpendicular to the long axis of the parallax ellipse, this method can be used to improve the precision of parallax measurements (and thus their useful range) by an order of magnitude. Spatial scanning also provides the means to obtain reliable photometry of the MW Cepheids, whose exceptional brightness would strongly saturate *HST* detectors in the briefest possible exposures with conventional imaging.

We have initiated three approved programs to collect an additional 18 sets of parallax measurements (GO 12879/13344 and 13334) and *HST*-system photometry for these and other Cepheids (GO 13335). Here we demonstrate these techniques from a pilot program of spatial scanning observations of the MW Cepheid SY Aurigae at an expected distance of about 2 kpc and from calibration observations of the open cluster M35. In §2 to §2.4 we describe the use of spatial scanning data to measure high precision, relative astrometry at a single epoch. §2.5 describes algorithms used to combine multiple epochs of spatial scan data to measure time-dependent astrometry. §2.6 covers the use of the preceding products to measure parallaxes. In §3 we describe the use of spatial scans to measure the photometry of bright sources. In §4 we discuss future directions of spatial scanning observations.

2. MW Cepheid Parallaxes with Optical Spatial Scanning

2.1. HST as an Astrometric Platform

Owing to its superior angular resolution and relative stability, *HST* is a promising platform for obtaining high-accuracy relative astrometry for sources within its field of view. The theoretical limiting precision for the measurement of a point source is approximately its root-mean square (RMS) width divided by the signal-to-noise ratio (S/N) of the observation. The S/N in a normal exposure is limited by the number of photons that can be collected before saturation, typically $\sim 10^5$ for most imagers, thus suggesting a theoretical limit of about 0.1 mas per pointed observation. In practice, *HST* has so far been limited to a best-case single-measurement precision of ~ 0.3–0.4 mas (~ 0.01 WFC3-UVIS pixel; Bellini et al. 2011), both with the FGS and with its imagers.

There are several reasons for these limitations. With the most efficient imagers, light is discretely sampled in pixels with angular size ~ 40 and 50 mas (WFC3 UVIS and ACS WFC, respectively). Measuring the position of a source to better than $\sim 1\%$ of the pixel size has proved very difficult (Bellini et al. 2011); among the contributors to a noise floor may be zonal and temporal variations in the effective point-spread function (PSF), and small-amplitude irregularities in the geometric distortion which cannot reliably be calibrated with existing data. Any variations in the

jitter over the image—produced, for example, by instantaneous rotations of the telescope—will introduce an additional field variation of the effective PSF. With the FGS, measurements are not limited by pixel size, but they are carried out one star at a time, so stability of the telescope and of the focal plane is paramount; in addition, the limited rate at which photons can be collected with the phototube detectors also limits the achievable S/N independent of the source brightness.

2.2. Astrometry with Optical Scans

Many of the limitations of pointed observations can be overcome via a new observing mode with WFC3, spatial scanning under FGS control, developed for WFC3 in 2011 to obtain photometry during exoplanet transits. In this mode, the target field is observed while the telescope is slewing in a user-defined direction and rate (to a maximum of $7\farcs8$ s^{-1}). Up to $5''$ s^{-1}, the telescope can maintain FGS guiding at all times; for faster scan rates, the telescope must be controlled by gyroscopes, leading to a smoother but less accurate motion. Each source thus describes a "trail" on the detector (see Figure 1). In the simplest mode, the motion is straight and uniform, resulting in a straight trail with constant brightness (counts per unit length) after accounting for geometric distortion in the detector. The trails for all sources are parallel in the distortion-corrected frame. More complex "serpentine" scans are also possible and can be preferable for sparse fields or exceptionally bright targets (see §4).

Some of the advantages of this method are immediately obvious. The light from each source is spread over a much larger number of pixels, allowing a larger global S/N to be achieved for each source[1]. Furthermore, each long trail provides thousands of separate position measurements in the cross-trail direction, one for each pixel traversed, thus averaging out the impact of single-pixel and local irregularities. Scanning at an angle relative to the detector also provides sub-pixel sampling of the undersampled WFC3 PSF. Because the measurements are time-resolved (e.g., 25 pixels per second at a scan rate of $1''$ s^{-1}), the telescope jitter can be subtracted as a function of time, negating the impact of even large ($\sim$ 1 pixel) jitter events which are not uncommon. With spatial scans, we expect to routinely achieve measurement precision of one-thousandth of a WFC3-UVIS pixel (1 millipixel, or mpix, corresponding to 40 μas) or better.

The disadvantage of this method is that precise measurements can be made in only one direction at a time, the direction perpendicular to the scanning motion, as positions in the direction along the motion are blurred by the motion itself. Thus, a precise two-dimensional measurement of relative positions requires in principle two observations. It is advantageous to choose scans to occur along the parallel readout direction (i.e., the Y-detector axis), as this limits the dominant direction of imperfect charge transfer and its attendant smearing to occur along the direction not

[1]The original motivation for this mode was the ability to collect $> 10^8$ photons per source without saturation, thus allowing high-precision global and time-resolved photometry of bright sources such as stars with transiting exoplanets.

being measured. The much smaller effect of the *serial* charge transfer efficiency is addressed in §2.5.2.

The disadvantage of obtaining positional changes in just one dimension is minimal for the measurement of parallaxes, as the motion of interest takes place in a predictable direction. By choosing the scan direction appropriately, the measurement can be made for the dominant parallax component.

2.3. Designing the Observation

The main characteristics of the planned observations relate to the brightness of the source, the availability of reference stars within the detector field of view, and the desired timing of the observation vs. the allowed telescope roll angles. An unusually large degree of planning and simulating is needed to obtain useful observations in this mode.

As in all narrow-field astrometric observations, WFC3 spatial scan observations can only measure the *relative* parallax of the target—the difference between the parallax of the target and that of nearby reference stars. All stars in the field of view move along similar parallactic ellipses with the same shape, orientation, and phase because the apparent parallactic ellipse traced annually on the sky is simply the reflex of the motion of the Earth around the barycenter of the Solar System. However, the amplitude of the motion of each star (e.g., its semimajor axis) scales inversely with its distance from the Sun, and represents the parallax. Since the absolute pointing of each observation is not known to better than a few tenths of an arcsecond, only the *difference* between parallaxes of stars in the field can be measured to useful precision. [2]

For this reason, it is critical for the field to contain a sufficient number of reference stars with independent distance estimates to correct relative parallaxes to absolute. Our typical observations in the plane of the Galaxy measure between 50 and 200 stars in a field of $5\farcm \times 2\farcm7$ defined by scanning WFC3-UVIS. It is important to note that distant stars, such as K giants several magnitudes fainter than the target Cepheid, are especially valuable in providing a correction to absolute parallax. For example, if a reference star is at 5 kpc (thus a parallax of 200 μas), even a relatively crude estimate of its absolute magnitude, perhaps with a 0.3 mag error, leads to a 30 μas uncertainty in its contribution to the correction to absolute parallax. With several such stars (a typical field will have 2–10 at this distance or beyond) and the use of a comprehensive set of UV, Strömgren, broad, and NIR bands to estimate stellar parameters, the uncertainty in this correction is expected to

[2]This situation is different from that of a telescope with wide-angle capability, such as GAIA or *Hipparcos*, which can observe simultaneously stars in different regions of the sky separated by a "basic angle" of tens of degrees, which then follow parallactic ellipses having different shapes and at different phases. Absolute parallaxes can be determined with precise knowledge of the basic angle and its stability, but they can be sensitive to systematic uncertainties in these quantities. Thus, parallaxes measured from the wide and narrow-field approaches provide a useful test for systematic errors in either one.

be well below our target measurement precision of 1 mpix (40 μas). Nonetheless, the correction to absolute parallax is a critical feature of our program, and the related uncertainties will be discussed in §2.6.

The optimal duty cycle for observing utilizes an exposure time of 350 s, just long enough to dump the buffer containing the previous observation during the next exposure, and a scan length of $\sim 144''$, as long as possible while ensuring that both the start and end points of the scan are visible for the primary target within the $163''$ field of view. This combination allows the largest number of scans per orbit, 4 or 5 depending on visibility, and near-continuous observations, and it yields a fiducial scan rate of $\sim 0\farcs4$ s^{-1}.

While any filter may be used for scanning, it is best to use a filter which has low wavefront errors and that passes light where CCD fringing is low. The use of longer wavelengths and redder filters would degrade resolution and increase fringing. Working too far to the blue can severely undersample the PSF (by a factor of 2 at 4400 Å) and diminish the S/N of red giants, which provide the best calibration to absolute parallax. The throughput of the filter is an important consideration as it determines the S/N of the target within the limited, useful dynamic range (6×10^4 e^- pixel^{-1} to 3×10^2 e^- pixel^{-1}, about 5.5 mag). It is also advantageous to choose a filter with a well-calibrated geometric distortion field (Bellini et al. 2011), as this provides the source of initial transformation from detector coordinates to the sky. The *F606W* filter ($\Delta\lambda = 2300$ Å, $\lambda_0 = 5907$ Å) is an attractive choice which makes useful measurements at the fiducial scan rate for stars at $10.6 < V < 16$ mag. Stars at $D = 2$ kpc in this brightness range will have $-1 < M_V < 4.5$ mag. Red giants in this brightness range will be at $5 < D < 10$ kpc (all magnitudes are quoted in the Vega system).

Long-period Cepheids ($P > 10$ days, $-4 > M_V > -7$) within 3 kpc are more challenging parallax targets because they are very bright ($6 < V < 10$ mag) and thus would saturate in a broad-band exposure at the fiducial scan rate. In order to avoid saturation, either a faster scan or a narrower filter is needed, with the reduction in counts proportional to the inverse of the increased speed or the decreased filter width. Scans faster than $5''$ s^{-1} rely on less precise gyro guiding, and given the importance of maintaining a fixed scan direction, we prefer to avoid their use. In most cases, scans at a similar rate but employing a medium- or narrow-band filter—e.g., *F621M* ($\Delta\lambda = 631$ Å, saturation limit $V = 9.2$ mag) or *F673N* ($\Delta\lambda = 100$ Å, saturation limit $V = 7.2$ mag)—suffice to observe the Cepheids without saturation.[3]

However, in such observations there are typically too few (5–10) sufficiently bright stars that can be measured with enough precision to provide the desired target precision in the reduction to absolute parallax (based on the shot noise of the source, 20 μas precision requires ~ 1000 counts

[3]Accounting for the variation in the Cepheid brightness can be important in fine-tuning the saturation limit. Such fine-tuning requires knowledge of the Cepheid phase and use of highly constrained observing times. It is feasible to observe at $V < 7$ without saturation using faster scans and serpentine scanning to make effective use of the additional scan length available.

per row and a trail length of a few thousand pixels). Thus, we rely on a hybrid approach: shallow, narrow-band scans to measure the Cepheid and a few reference stars, followed by deep, broad-band scans to measure 50–200 distant reference stars. The stars bright enough to be measured in the shallow scan and yet faint enough to avoid saturation in the deep scan serve as a bridge between the target Cepheid and the bulk of the reference stars; for this purpose, we do not require any knowledge of their distance or motion. Since the broad and shallow scans are taken concurrently, there is no significant astrophysical motion of the reference stars between scans, and the uncertainties associated with long-term motions (e.g., parallax) are negligible in this step. However, linking together shallow and deep scans can be a significant component in the final parallax error budget, as discussed in §4.

2.4. Analysis of Scan Data

Figure 1 shows a typical scan image for the SY Aur field. (See Table 1 for a listing of scanning observations of SY Aur.) The nearly vertical "trails" are the images that each star leaves as the telescope scans over $144''$, 88% of the length of the field of view. The area covered by the scan is almost twice the normal field of view of the camera. Stars near the center of the region spanned in the detector Y direction will have trails that start and end within the frame, while stars farther from the center have trails that enter or leave the frame during the scan. Cosmic rays are the only compact sources in the frame and are readily identified by their lack of vertical extent, allowing us to disregard impacted pixels.

2.4.1. The M35 Calibration Program

As part of the WFC3 calibration program, multiple scan observations were obtained in *HST* program 13101 for a field covering part of the open cluster M35 at two orientations 180° apart, using the filters *F606W*, *F621M*, and *F673N*. See Table 1 for a listing of these observations. Owing to its position very close to the ecliptic plane, M35 can be observed at nearly constant telescope roll angle for several months, and it reverses available roll within a few days of its antisun position. It also includes 40 stars of nearly optimal brightness ($10 < V < 17$ mag) for observations in the selected filters. This combination of properties makes it an ideal target for calibrating spatial scan astrometry and in particular parallax observations, which also require observations at orientations differing by 180°. The stars in M35 have a small velocity dispersion of $0\farcs02$ per century ($0.5\,\mu$as per day), so the few-week interval between observations at orientations that differed by 180° produces ~ 0.25 mpix of dispersion; thus, the relative positions of the stars can be treated as being static within the calibration data. At each of two epochs a sequence of 350 s scanning frames of the M35 field were obtained back-to-back, 10 for *F606W* and 5 each for *F673N* and *F621M*, to better understand the effect of the orbital thermal cycle and 180° orientation change on relative positions. We will refer to a number of results derived from the analysis of the M35 data in the following

sections.

2.4.2. Matching Trails to Stars

The first step in the analysis of scan data is the identification of the trail positions and of the stars associated with each trail. Using a catalog of star positions obtained from direct WFC3-UVIS images, the start and end positions of star trails can be predicted from the scan location and its velocity vector. Small adjustments are needed to precisely align the direct and scan images, whether both are obtained at the same epoch or not.

It is also necessary to identify and catalogue stars with trails that overlap trails to be measured. We refer to these contaminating sources as "spoilers," as they can throw off subsequent position measurements. We identify the regions within each star's trail that are affected by spoilers, and disregard the impacted pixels. Tests show that spoilers are significant if the stars differ by < 7 mag and the trails lie within 8 pixels of each other.

2.4.3. Minirow Fits

The next step in the analysis process is measuring the cross-scan position of each star as a function of position along the trail. For each trail, we extract the pixel values and quality flags at each integer pixel step along the trail within ± 10 pixels ($\pm 4\times$ the full width at half-maximum intensity) of the nominal trail center. We call this individual block of information a "minirow," as it is a small part of the detector row where signal from the star of interest is located (see Figure 2). Individual trails may be composed of a few hundred to several thousand minirows. [4] Each minirow thus consists of a short (typically 21 pixel) array of data values vs. X pixel location at a fixed Y location. Each pixel is also assigned a weight based on the detector noise model including zero weight for bad pixels; pixels too close to a spoiler are given zero weight, and if pixels within ± 2 pixels of the peak are rejected, the minirow is rejected as being invalid. The fit involves three parameters: the amplitude, or scaling factor for the line-spread function (LSF), which sums to unity over its full length; the center position, or amount by which the LSF must be offset and spline-interpolated along the detector X direction for an optimal match; and the background, or constant level that must be added to the line profile to match the data. The LSF, oversampled by a factor of 4, is previously derived as a function of X and Y detector position from the empirical PSF in images of star clusters (Bellini et al. 2011). Positional uncertainties are determined from the χ^2 of the minirow fit with a minimum floor of 0.01 pixel imposed at 10^4 e^- pixel^{-1} to reflect the finite precision of the geometric distortion field obtained from (Bellini et al. 2011).

[4] We discard trails with fewer than 300 available minirows, as their astrometric fit will generally suffer in both statistical value and systematics from the small coverage.

2.4.4. Position in Rectified Coordinates

For each trail, the minirow fits yield a number of (Y, X) pairs representing the fitted X position in detector space at the Y detector location. In order to proceed with the analysis, we need to transform these (Y, X) positions into a reference frame in which they are directly comparable; for example, we expect the trails from different stars to be essentially parallel, with their perpendicular (across scan) separation constant; this is not true in detector coordinates, which suffer from a variable geometric distortion. In addition, portions of the trails in Detector 1 cannot be readily compared to those in Detector 2 without a global distortion solution.

We use the field distortion solution from Bellini et al. (2011), which uses a definition of the PSF position that is consistent with the empirical determination of the PSF. Whatever the definition of the PSF position (e.g., centroid, center of symmetry, peak), it is crucial that it coincide with the derivation of the field geometric distortion. *From here forward our analysis utilizes pixel positions on the sky unless explicitly stated otherwise.*

The geometric distortion solutions have an accuracy of ~ 0.01 pixel on scales of ~ 40 pixels (Bellini et al. 2011). This accuracy is sufficient to reach position precision of 1 mpix (40 μas) for full-length scans, which would be a significant contribution to our overall error budget. In addition, the thermal cycle of *HST* within an orbit (also known as telescope "breathing") and temperature variations due to the recent attitude of the telescope changes the focus position by $\pm 5\mu$m during the orbit, which can cause the optimal geometric distortion solution to vary. Although a thermal model of *HST* is available to predict these variations, the optical model of the telescope does not have enough fidelity to allow a useful correction of the geometric distortion field. An improved geometric solution which takes into account its possible variability is necessary to achieve our measurement goal. In the following sections we show how a combination of internal and self-calibration can be used to reduce the impact of the geometric distortion below $\sim 20\,\mu$as.

Annual variations in Earth's velocity vector induce changes in plate scale which can be treated as a simple isotropic scale term for our narrow field. Typical values of the velocity aberration are of order 10^{-4} from the ± 30 km s^{-1} Earth velocity, requiring a scale correction of ± 200 mpix from the frame center to the edge. Variations in spacecraft velocity during a scan result in variations in the velocity aberration which can reach a peak of 6×10^{-6} or ± 10 mpix. This velocity aberration correction, proportional to the combined velocity of the telescope and Earth with respect to the Solar system barycenter, projected along the line of sight to the target, is computed on the basis of the *HST* ephemeris as part of the standard pipeline image processing, and is stored in the header of each image. We apply a simple sinusoidal interpolation to the recorded values in order to obtain the *instantaneous* scale correction for each minirow—the value depending on the time attached to that minirow, or equivalently, the time at which the star was traversing that specific pixel location. All position measurements are scaled according to the instantaneous velocity aberration that applies.

2.4.5. Jitter and the Reference Scan Line

A feature that is immediately apparent from the values of the fitted X position vs. position along the scan (see Fig. 2) is that the values vary locally much more than the estimated error in each measurement, with variations of ~ 0.1 pixel and occasional jumps of up to 1 pixel. Comparing different trails at equivalent positions along the scan (e.g., at the same distance from the start of the scan), as shown in Figure 3, reveals that these variations are highly correlated from star to star, and are in fact caused by irregularities in the telescope motion—equivalent to the so-called "jitter" in pointed observations. Unlike pointed observations, for which the jitter produces a modest blurring of the PSF, scanned observations can be used to measure and correct for the telescope jitter perpendicular to the direction of motion (our preferred measurement axis). In addition, the presence of jitter allows a more accurate measurement of the relative position of each star *along* the scan direction, from a template fit or cross-correlation of the jitter features. Each star will be affected by different jitter features, depending on where it is located in the field of view and thus for what fraction of the exposure it is on the detector; to avoid systematic offsets due to asymmetric jitter, it is thus necessary to correct for the jitter at the pixel-by-pixel level.

For this purpose, we define a *reference scan line* from the weighted average of all stars. The reference scan line represents the instantaneous offset from the ideal rectilinear motion of the telescope as a function of position along the scan (which is a proxy for time). A proper definition of the reference scan line requires accurate (< 0.25 pixel) knowledge of each star's position along the scan direction, to avoid blurring of jitter features. We carry out this process iteratively. We obtain a first approximation to the reference scan line from the along-scan position determined either from a star catalog or from the apparent start/end position of the trail; these are typically accurate to ~ 1 pixel. Then we fit this approximate reference scan line to each trail, thus obtaining a better position along the scan, and produce a new reference scan line from the updated positions in rectified pixel space. The final reference scan line is oversampled by a factor of 4; for the best-measured trails, the estimated uncertainty in the along-scan position is a few percent of a pixel, sufficient to resolve the jitter frequency. Figure 3 shows the comparison of bright star trails aligned in scan time and the residuals after subtraction of one from another.

2.4.6. Trail-to-Trail Separation Along the Scan: Variable Rotation

One fundamental assumption of the scan method is that trails for different stars are essentially parallel, so their separation remains constant (on the sky, after correcting for geometric distortion) throughout the observation. On short time scales (< 1 second), the parallelism of trails is demonstrated by the correspondence of their jitter features. However, on longer time scales ($\gtrsim 1$ minute, corresponding to several hundred pixels traversed), the separation of trails occasionally appears to vary by several mpix—difficult to measure individually, but quite apparent in a statistical sense. Initially we investigated the possibility of deviations from the nominal geometric distortion;

however, this interpretation would require that the deviations be repeatable across observations of different fields, which turns out to be inconsistent with the properties of the calibration data obtained for M35. Instead, the nonparallelism of trails exhibits a pattern consistent with slow rotations of the telescope's field of view (equivalently, its roll angle) throughout the observation. Under this interpretation, a single parameter—the instantaneous differential roll angle—causes small changes in the separation of each pair of trails in a pattern strictly dependent on their relative separation in the scan direction. Figure 4 shows the scan patterns formed by fixed or variable field rotation. Indeed, solving for a slow variation of the telescope roll angle (typically fitted as a fifth-degree polynomial in position along the scan, a proxy for time) removes the variation in separation between trails below statistical significance. Empirically, the instantaneous roll angle changes by 0.001° to 0.003° over an observation.

The most likely reason for a variation in the instantaneous roll angle is in imperfections of the geometric solution in the FGS. Under FGS control, the telescope tracks the position of the guide stars throughout the observation, and makes continuous roll adjustments on the basis of their position in the focal plane to ensure that the roll angle remains constant. However, this requires very good knowledge of the geometric distortion solution in both FGSs over the more than $2'$ that each guide star traverses during a scan. A local error of ~ 0.5 mas over $30''$ would suffice to explain the observed changes in roll angle. Crucially, we observe that the variation in roll angle is consistent across observations of the M35 field, regardless of filter, direction, and time of the scan; however, different fields, or observations of the same field at different roll angles (which changes the position of the guide stars within the FGSs), have essentially a different but again internally consistent set of variations of roll angle. Both of these properties are consistent with the FGS geometric distortion interpretation (Nelan 2012).

In practice, we determine the change in roll angle as a function of position along a scan field using an average obtained from deepest scans of that field. The mean is then applied to all scans of this field. This is especially helpful for shallow scans whose trails lack the precision necessary to effectively quantify the variations in roll during the scan.

The result of the analysis of each scan image *treated individually* is a set of position measurements for each star in the nominal X direction. These measurements are with respect to the reference scan line defined after the correction for variable roll. The position of the reference scan line is arbitrary; there is information only in the *relative* position of the stars with respect to one another.[5] Each measurement is also associated with its estimated error, and several ancillary quantities are recorded for each trail, including the number of valid minirows, typical amplitude and χ^2, and the position of the trail on the detector.

By measuring stellar positions at three or more epochs at six month intervals, we may now

[5]The absolute pointing precision of *HST* with respect to an inertial reference system is several orders of magnitude less accurate than the precision goal of this project.

determine the proper motion and parallax of the measured stars.

2.5. Using Multiple Observations at the Same Epoch

For some applications of astrometric measurements it may be beneficial or even necessary to first combine the measurements of multiple scans obtained at a common epoch. Applications include combining multiple scans to reduce sources of error, combining scans obtained under different conditions to calibrate the effect of the conditions on measured positions (e.g., thermal state), or combining scans of differing depth to improve the dynamic range of the measurements. In applications for which the target and reference stars can be well measured at a single exposure depth (i.e., a range of ~ 5 mag), one can proceed directly to measuring parallax in §2.6.

2.5.1. Bridging the Dynamic Range Gap for Cepheids

Because of the large difference in brightness between Cepheids and field stars, typically 4–10 mag, it may be necessary to obtain shallow and deep exposures at the same epoch and combine their measurements. To obtain high-quality measurements at the fiducial scan speed for reference stars in the range $11 < V < 17$ mag, a depth where they are plentiful, *F606W* is the filter of choice, with a typical field providing 50–200 such stars with a full-scan uncertainty $< 50\,\mu$as, sufficient to control the uncertainty associated with the reduction to absolute parallax addressed in the next section. A narrower filter—e.g., *F673N* or *F621M*—is then used to obtain an unsaturated trail for a bright Cepheid with $V < 10$ mag; however, in shallower scans most reference stars are too faint to provide a good anchor to spectroscopic distance estimates and thus a reduction to absolute parallax.

Our solution for SY Aur ($8.6 < V < 9.4$ mag) is to obtain a pair of scanning observations in both *F606W* and *F673N* within the same orbit, during which the stars can be assumed to be stationary. The shallow observations in the narrow-band filter yield a full-precision measurement for the Cepheid (indeed, we may choose the filter and scan speed so as to maximize the electrons collected from the Cepheid while avoiding full-well saturation) and good measurements for ~ 5–10 other stars of intermediate brightness in the field. The intermediate stars anchor the shallow frame to the deep frame, and thus tie the Cepheid motion to the reference frame defined by the collection of reference stars. We call this step "aggregation"; it results in position measurements for all stars, including the Cepheid, in a consistent epoch-based reference frame. Errors are also reliably estimated from the aggregation step, with contributions from the scan measurements and nuisance parameters used to combine scans, and the resulting measurements at each epoch form the basis for the parallax and proper-motion measurements described in the following section. Note that a dearth of intermediate brightness stars can lead to degradation of the Cepheid parallax, as discussed in section §3.

2.5.2. Single-Epoch Position Measurements

The goal of the aggregation step is to obtain for each star a single measurement of position perpendicular to the scan direction that optimally uses all the measurements obtained at the same epoch.

The aggregation step uses a model relating the "true" position of each star in the measurement direction to its measured position in each scan. Each star has one free parameter, its nominal position in the measurement direction; in total, there is one fewer parameter than stars, as our position measurements are *relative*, and thus insensitive to a bulk shift of all positions in the measurement direction. As a convention, we take the mean of the true positions of all stars observed in the field to be zero to set the arbitrary reference position. The true positions of N stars are thus described by $N-1$ positional parameters.

In addition to the parameters describing the stars' true positions, the transformation from true to observed position involves several additional effects that need to be quantified and modeled. The most obvious ones are scan-to-scan offset and field rotation as discussed in §2.4.5 and 2.4.6. The offset is a free parameter for each scan, as the absolute telescope pointing is not stable enough to constrain its scan-to-scan position to the required accuracy of tens of μas. The roll angle of the telescope is not identical for scans with the same requested roll angle, and small variations ($< 0.001^\circ$) need to be taken into account. Both offset and rotation are defined with respect to the first scan by convention; thus, aggregating M scans requires $M-1$ offsets and $M-1$ rotations.

Analysis of the M35 data, seen in Figure 5, shows clearly that these two parameters are not sufficient. Residuals between model and measurements routinely reach 5–10 mpix, even for scans that are obtained in the same filter and orbit in succession, well in excess of the expected statistical measurement errors. Furthermore, such residuals, as shown in Figure 5, have clear spatial correlations that indicate that there is variable low-order distortion at the few mpix level. The residuals are somewhat greater between different filters, largely due to a static scale difference, and between observations obtained at different orientations, as these include both the previous variable term as well as errors in the static geometric distortion field. These residuals do not show any correlation with the sources' brightness or color, and thus are most likely related to variations in the geometric transformation between true and measured positions.

For the M35 calibration data, a successful approach consists of including in the model a low-order polynomial correction with free coefficients for each observation (see Fig. 5). We adopt a polynomial correction to the X coordinate when aligning two frames which depends on the pixel position of each star trail in the detector; the assumption is that any variation in the transformation from true to measured position is tied to the telescope and detector, and therefore is best described in measured rather than true coordinates. Note that a generic first-degree polynomial includes by definition an X scale term (the first-order correction in X) as well as a *detector* rotation, which is slightly different but closely related to the *field* rotation previously considered.

We find that a second-degree polynomial as a function of X and Y coordinates is adequate to describe the X coordinate transformation between two scans and reduce residuals of well-measured stars to $\lesssim 1$ mpix, as shown in Figure 5. (Only terms of *total* degree up to the polynomial degree are included.) Figure 5 shows the residuals after these polynomial corrections are included in the model. A second-degree polynomial in X and Y has five coefficients and the transformation has a total of seven parameters, including rotation on the sky and a constant term. The leading polynomial term of the cross-filter match has degree (1,0), corresponding to an overall scale factor, and indicates that the geometric solution we initially adopt has a scale in *F673N* that is about 1.5×10^{-5} different from the *F606W* scale, or up to 40 mpix near the edge. Several other terms also have significant power but generally vary in sign, with contributions of up to 50 mpix at the edge of the field. Not surprisingly, the coefficients of these terms are smallest when a pair of frames have a similar predicted time-dependent focus position of the telescope based on the *HST* orbital thermal model as shown in Figure 5. Thus, it appears that much of the role of the polynomial correction is to account for PSF and field distortion caused by the changing thermal state of *HST*.

To quantify the size of a color dependence of the geometric distortion (i.e., a color wedge) over the broad range of the *F606W* filter, we used the M35 data to compare the relative source positions in *F673N* and *F606W* versus the $B-V$ color after accounting for variable distortion. The full color range of the stars was $-0.15 < B-V < 1.4$ mag, with a mean color of 0.57 mag. We assume that any color effect in *F673N* is negligible owing to its very narrow wavelength range ($\Delta\lambda = 100$ Å vs $\Delta\lambda = 2300$ Å), so the dependence on color is a measure of a chromatic term in *F606W*. We find a very small color shift from the M35 data of 0.6 ± 0.2 mpix for an 0.5 mag difference in color from the mean. Eliminating the two bluest stars with $B-V < 0$ mag reduces the effect further to -0.1 ± 0.2 mpix and is more appropriate for the colors encountered for field stars and Cepheids. Given the small empirical size of a chromatic shift and the fact that Cepheids lie near the middle of the color range of stars, we conclude that a chromatic effect in *F606W* is negligible, and we will explore additional chromatic effects with an expanded dataset in the future.

In principle, imperfect charge-transfer efficiency (CTE) can smear charge along the readout axes and shift astrometry. The effect is 1–2 orders of magnitude smaller along the X axis for *HST* CCDs owing to the greatly reduced pixel transfer (and trapping or detrapping) time than for the Y axis. For this reason we chose to scan observations along the Y-axis and measure astrometry along the X-axis. However, a small amount of charge is apparent trailing hot pixels in the X axis opposite the read direction indicating the presence of short timescale charge traps and imperfect X-CTE. This deferred charge is about 0.08% for a pixel with 10,000 electrons and becomes a smaller fraction for brighter pixels. The resulting astrometric shift is about twice as large for a given charge total in a 2 dimensional PSF than the 1 dimensional minirow of a scan due to the larger shift affecting the fainter PSF wings. Using these calibrations, we estimate the shift of SY Aur in the shallow scan from fast trapping would be ~ 0.4 mpix and even smaller, about < 0.2 mpix, for a Cepheid with peak counts of $> 30,000$ electrons. Depending on the relative position of stars and amplifiers across epochs, the effect on a star's measured parallax may fully or partially cancel. For SY Aur

we conclude that the effect ($< 3\%$ at 2 kpc) can be neglected. In the future we will try to directly measure the change in scan line astrometry in the X-direction by dithering a source back and forth across the line dividing the read-out X-direction for use in a larger sample analysis.

For the SY Aur field we observed the Cepheid at $8.7 < V < 9.4$ mag in *F673N* at the fiducial scan rate of $0\farcs4\,\mathrm{s}^{-1}$, resulting in peak counts for the Cepheid of 10,000–15,000 electrons, thus providing unsaturated measurements to complement the contemporaneous *F606W* scans (where the Cepheid is oversaturated by a factor of 5–6 and *F621M* would saturate by a factor of 1–1.5 if used). Unfortunately, the anti-galactocentric direction of SY Aur (Galactic longitude $\ell = 164.75°$) results in a rather sparse field with only three stars that are both well-measured in *F673N* ($7 < V < 13$ mag) and not saturated in *F606W* ($V > 11$ mag). Because the calibration requirements to reach millipixel precision from spatial scanning were not known at the start of this pilot project, the selected field of SY Aur is less than optimal.

A few more stars exist at $13 < V < 15$ mag, providing a little additional constraining power. The paucity of stars available to define the transformation between the shallow and deep frame results in a relatively noisy mapping which is not very robust. While the mean precision of each Cepheid position measurement in *F673N* is 0.4 mpix (see Fig. 6), transforming the unsaturated Cepheid position in *F673N* to *F606W* with so few stars degrades the Cepheid position to about 2 mpix precision. As shown in Figure 6, for other Cepheid fields selected in directions richer with reference stars, we find that we can constrain the Cepheid position in the deeper scan to 1 mpix.

2.6. Multiepoch Combination and Parallax Fit

The final step is to utilize the multiple measurement epochs taken over the course of two years at intervals of six months, in order to estimate the parallax and proper motion of each star in the field. This model involves several considerations. First, the position of the stars in the field, relative to one another, naturally changes over time as a consequence of their astrometric motion *in the measurement direction*. This motion is modeled as the combination of a linear term, which is the projection of the proper motion along the measurement direction, and a periodic term, which is the projection of the parallactic motion. Note that the shape and phase of the parallactic motion as well as the component in the measured direction are fully known from the position of each star, the motion of the Earth with respect to the barycenter of the Solar System, and the orientation of WFC3; the only free parameter is its amplitude, which scales directly with the parallax of the target. Thus, the standard astrometric model involves three parameters for each star: position, parallax, and proper motion along the measurement direction.

Observations spaced every half year, at the time of the maximum and minimum parallactic excursion, give optimal discrimination between parallactic and proper motion. In practice, *HST* observations of SY Aur could be scheduled at the optimal time (mid September and early March) at an orientation no closer than 35° (or $180 + 35°$) from the optimal, reducing the apparent parallax

component to 80% of its maximum value. The available roll angle at a given time depends on *HST*'s orientation with respect to the Sun (in relation to the telescope aperture and solar panels) and the availability of guide stars. Although the observation orientation may not be optimal, symmetry ensures that the same orientation flipped by 180° will be available 6 months later.

At least three epochs are necessary to be able to disentangle parallax and proper motion for each star. In practice, three epochs will not suffice; additional free parameters are involved in registering the observations, and the errors in the derived parameters would be much larger than the measurement errors. Four epochs are in general sufficient to obtain good constraints on the parallax and proper motion separately; when available, five epochs help reduce the covariance between derived parallaxes and proper motions, and improve the precision of the final measurement beyond the obvious factor $\sqrt{5/4}$. For SY Aur we have in fact five epochs, although two lack repetition of the shallow or deep scan.

In addition to the astrometric parameters of each star, the model includes geometric parameters used to align each epoch with one another (offset and rotation), as well as any residual large-scale adjustment to the geometric distortion required to reduce the model residuals. This last part is identical to the single-epoch aggregation step in §2.5.2, but it now substitutes the stationary star assumption with the astrometric model for each star. We also now utilize epochs obtained with orientation differences of 180°.

The full model can be formally described by the expression

$$X_{ij} = X_{i0} - X_{\mathrm{ref,j}} + pmx_i\,(t_j - t_0) + \pi_i\,f_j + R_j\,Y_{i0} + \langle P(X_{\mathrm{det}}, Y_{\mathrm{det}})\rangle_{\mathrm{trail,ij}} \qquad (1)$$

Here the basic measurements are the positions X_{ij}—that is, the X position of the trail of star i in image j (relative to the reference scan line), measured after correction for variable rotation, scale-corrected for velocity aberration and variable distortion, and projected onto a constant sky frame. The X coordinate is aligned with detector X and, by design, aligned with the bulk of the parallactic motion. The quantity X_{i0} is the reference position of star i at time t_0, and $X_{\mathrm{ref,j}}$ is the offset of image j in the X direction—in essence, the position of the reference scan line for image j on the sky. The astrometric motion of star i in the X direction is described by the X component of the proper motion, pmx_i, and the parallax π_i, applied with the epoch-dependent parallax factor f_j. The term f_j is the projection (for unit parallax) of the parallactic motion in the X direction at the time of the observations. Note that the proper motion can only be relative, since any change of all proper motions by the same amount can be subsumed into a change of $X_{\mathrm{ref,j}}$ for each epoch. As far as the astrometric model is concerned, parallaxes are also relative; however, the degeneracy in the conversion to absolute parallaxes can be broken by using spectrophotometric distance estimates for the stars in the field. Finally, the model position must be corrected for the relative rotation and geometric distortion of image j with respect to the reference image. The rotation term on the sky is $R_j\,Y_{i0}$, where R_j is the rotation of image j and Y_{i0} is the static relative position of star i in rectified coordinates along the Y direction with respect to the center of the field. (Since

typical rotations are of order 10^{-5}, a measurement of Y_{i0} with a precision of ~ 1 pixel will suffice.) The polynomial term is determined as part of the model-fitting procedure, typically as a second- or third-degree polynomial $P(X_{\rm det}, Y_{\rm det})$, where $X_{\rm det}$ and $Y_{\rm det}$ are detector coordinates; the total correction is determined by evaluating the polynomial at every location along the trail of star i in image j and averaging the result. By convention, the rotation and polynomial term apply to each frame in relation to the first in a set.

Again, the M35 calibration data provide good guidance, as they were obtained at two orientations which differed by 180°. These data are useful for defining a family of polynomials with the smallest number of terms needed to adequately account for variable distortion (at the same orientation) or static and variable distortion (at flipped orientation).

In the final step we need to convert the relative parallaxes into absolute, thus yielding a geometric distance estimate. This is accomplished by estimating the reference star parallaxes from the spectrophotometric absolute magnitude estimates that come from multiband photometry and medium-resolution spectroscopy. The distance estimate of the target star will be insensitive to uncertainties in the distance of the reference stars so long as the set contains objects which are bright and distant (e.g., red giants).

For the SY Aur field (and for other Cepheid fields in progress), we obtained direct imaging with *HST* during the scanning observations and measured photometry of all reference stars in the UV (*F275W*,*F336W*), Strömgren (*F410M*,*F467M*,*F547M*), and broad-band (*F850LP*) systems. To this photometry we added J, H, and K-band photometry from the 2MASS survey to provide a set of up to 9 bands of photometry from 0.2 to 2.2μm. All the photometry was of high S/N, with the exception of *F275W* where only a third of the stars yielded a measurement ($F275W < 22.8$ mag). Missing or excluded photometry was recorded for stars which suffered cosmic ray hits, suffered blending in the 2MASS data (as identified with *HST F850LP* imaging), and for half the field not covered by *F410M* imaging. In practice, the average number of bands with useful measurements per star was between 6 and 7.

To estimate the spectroscopic parallax for each reference star, we generated a sample of 29,000 mock stars in the direction of SY Aur using the Besançon galaxy model (Robin & Crézé 1986; Robin et al. 2003, and references therein). The thick disk of the model has been updated to better fit SDSS and 2MASS data (Robin 2013, private communication).

This sample of mock stars has a distribution of the four parameters ($\log g$, initial mass, metallicity, and extinction), as expected from the Besançon model along the sight line to SY Aur. The extinction to the edge of the Galaxy is defined from Schlegel et al. (1998). For each mock star we select the stellar model from the Padova isochrone tables (Bressan et al. 2012) whose parameters best match the mock parameters. [6] Each stellar model includes a determination of the absolute

[6]The zeropoints of the Padova isochrones are themselves based on geometric distances by the use of *Hipparcos* parallaxes of nearby stars and the use of eclipsing binaries to measure masses, and thus are unlikely to have a

magnitude (including the mock extinction appropriate for each band) of that model star in each of the measured bands, thus producing 29,000 mock stellar models. The comparison of each mock model to the measurements of a reference star produces a distance estimate (and an estimate of the 4 nuisance parameters) and a likelihood that the model is good based on the size of the χ^2 statistic between model and data.

We independently determined the temperature and luminosity class of the majority of the reference stars via medium-resolution optical spectra compared to template spectra. The spectra were obtained with the Kast double spectrograph (Miller & Stone 1993) on the 3 m Shane reflector at Lick Observatory and DIS on the APO 3.5 m. Standard procedures were used for the data reduction.

In order to combine the photometric and spectroscopic results, we treated the spectroscopic term as an additional contribution to the χ^2 statistic on the basis of the agreement between the temperature and the $\log g$ term given for the best-matching spectral template, including both spectral and luminosity class. The spectral templates used were from (Pickles 1998) and the ELODIE database (Prugniel & Soubiran 2001). This is especially important for discriminating dwarfs from giants, for which the spectroscopic contribution is often more powerful at discrimination than photometry. Each star's distance (and expected parallax) was determined from the normalized, summed product of mock distances and likelihoods (i.e., the Bayesian mean), with uncertainties fixed at 0.3 mag as derived from Monte Carlo simulations of the models. The parallax uncertainty (i.e., systematic uncertainty in frame parallax) of the set of 31 fitted reference stars is 12 μas, well below our target uncertainty. As expected, most of this precision comes from the most distant stars which are primarily red giants. A single red giant at a distance of 5 kpc would give an uncertainty of 30 μas. Indeed, the five most distant stars alone give an uncertainty in the reduction to absolute parallax of 18 μas, equivalent to three distant red giants. Assuming a larger per-star uncertainty of 0.5 mag increases the uncertainty in the constant parallax term to 21 μas, still well below our overall accuracy for this field. These estimates allow us to break the degeneracy between relative parallaxes and obtain an actual parallax estimate for each star, including the Cepheid.

2.6.1. Setting Up the Model

In practice, the modeling process attempts to reproduce the relative epoch-to-epoch position measurements for each star on the basis of three parameters for each star: the position at the first epoch, the parallax, and the proper motion. One position and one proper motion are fully degenerate; for simplicity, we assume that the mean position at the first epoch and the mean proper motion of all stars considered both vanish, but no result (except for a constant offset in the proper-motion terms) depends on these assumptions. Another way to say this is that we have no ability to

---

considerable, systematic error in distance scale

establish a precise reference system for either position or proper motion from the data available to us. Each epoch after the first is allowed a rotation, a constant term, and a second-degree polynomial adjustment to match the first epoch; since there are about 34 stars useful for measurement at each epoch, these additional 7 parameters per epoch over which we marginalize do not place an undue burden on the solution.

In addition, we use the *a priori* distance estimates based on spectrophotometric parallaxes as priors for the parallax of the stars in the field. A prior is not used for the Cepheid, so that its distance estimate is determined directly from its observed parallax.

The best values of the model parameters are determined using a version of the Levenberg-Marquardt algorithm which includes proper error propagation of the model uncertainties. Among these parameters is the *absolute* parallax of the target Cepheid, which then provides the distance and error estimate for SY Aur. A modest fraction of the reference stars in the field are expected to be part of binaries with parameters that would cause a significant deviation from our simple astrometric model. This fraction depends on distance and spectral class, but is $\sim$ 10–20% for F and G stars at 1 kpc on the basis of the distribution of binary properties in Duquennoy & Mayor (1991). We run the global model iteratively after rejecting outliers on the basis of their disproportionate contribution to the total χ^2; this results in the rejection of 8 reference stars.

2.6.2. Multiparametric Model for SY Aurigae: Results

The resulting fits for the SY Aur field are shown in Figure 7. For the remaining 26 reference stars, the spectroscopic parallax constraints are shown, compared to the *a posteriori* parallax. The proper-motion estimates are subtracted from both data and model for ease of examination. For bright stars with long scans, the parallax uncertainty is just under 40 μas, sufficient for a 16% measurement of parallax for two red giants, stars 4 and 10 at $D = 3.4$ and 4.1 kpc, respectively. The distance of the Cepheid SY Aur from its parallax is $D = 2.3$ kpc, making this star and others in the field the most distant stars with well-determined parallax. This distance is in good agreement with the expectation of $D \approx 2.1$ kpc based on the Wesenheit P–L relation of Cepheids (Tammann et al. 2003).

The precision of the Cepheid parallax at this distance should be about 4% based on optimal photon statistics, a designed 3600-pixel-long scan length, and position in the center of the field away from larger and more uncertain distortions at the edge of the field. Because this particular Cepheid at $8.8 < V < 9.4$ mag is too bright to avoid saturation in the deep scan when $V < 10.6$ mag, its measurement precision would be lower, about 6%, owing to the reduced photon statistics in the shallow scan. However, the lack of bright stars in this field (only 3 with astrometric errors of $< 100\,\mu$as in the shallow scan; see Fig. 6) degrades the precision of the transformation between the shallow and deep scan for the Cepheid to between 50 and 100 μas and thus the precision of this parallax to 12%. Through better understanding of the parameters which affect the parallax

precision, we selected better Cepheid fields for new observations with more reference stars, as well as filters and scan speeds which maximize photon statistics, to get much closer to the attainable precision (see Fig. 6). In addition, the precision of the SY Aur parallax from these data should improve through better empirical knowledge of the spatial transformation between WFC3-UVIS filters garnered from ongoing spatial scans of other Cepheid fields, so we consider this measurement to be preliminary until collection of the full-sample of 19 Cepheids.

3. Bright-Star Photometry

3.1. Spatial Scanning Photometry

While ground-based observatories have imaged these bright MW Cepheids in the NIR, systematic uncertainties in the flux scale between the ground and *HST* photometric systems would limit the precision of the Hubble constant independent of the measurement of their parallaxes. The long-term internal stability of the nonstandard *HST* photometric system in the NIR has been established to $\sim 1\%$ (Kalirai et al. 2011). However, the NIR *HST* WFC3-IR bandpasses of *F160W* and *F125W* used to observe Cepheids are not well matched to ground-based bandpasses, which are set by natural breaks in atmospheric OH emission and water transmission. The difference between a typical ground-based H-band filter and its WFC3-IR equivalent, *F160W*, is large, with color terms demonstrating a 20% difference between the measured brightness for stars with $J - H$ differing by 1 mag. In addition, ground-based systems suffer from photometric instabilities at the few percent level owing to nightly and hourly variations in the amount of precipitable water vapor and aerosols in the atmosphere. The best-understood NIR ground-based system, 2MASS, is calibrated to a precision of 0.02–0.03 mag (Skrutskie et al. 2006). Not surprisingly, systematic differences of 0.02 mag exist between the mean NIR magnitudes measured for *the same Cepheids observed at different ground-based observatories*, even after accounting for the known differences in their photometric systems (Monson & Pierce 2011). These remaining differences likely reflect the limitations with which the throughput of any ground-based system is known in the NIR and present a critical *systematic* uncertainty in relating ground-based NIR magnitudes of MW Cepheids to those in distant galaxies observed with *HST*.

While optical ground-based and *HST* systems are easier to cross-calibrate than those in the NIR, even the uncertainty between these systems resulted in a reported 5% systematic uncertainty in the determination of H_0 by Freedman et al. (2001).

The only way to ensure that future highest-quality Cepheid parallaxes from *HST* or GAIA are fully leveraged is to observe the nearest MW Cepheids with *the same photometric system used to observe their distant counterparts.* However, it is challenging to accurately measure the brightness of nearby, long-period Cepheids with *HST*. The 33 known MW Cepheids with $P > 10$ days and $D < 5\,\mathrm{kpc}$ have $3.5 < H < 7.5$ mag and $6 < V < 10$ mag, and any would saturate in the shortest exposures possible with WFC3-IR in the *F125W* and *F160W* filters. In addition, the

shortest possible exposure, 0.1 s with the smallest subarrays (unsaturated for $H > 8$ mag), limits the aperture radius to 32 pixels ($\sim 4''$), which is not ideal for distinguishing the sky level from the wings of the PSF. While it is possible to accurately measure saturated sources by fitting to the unsaturated wings of the light profile, it is important to minimize the degree of saturation, as exclusive reliance on pixels progressively farther out in the wings increases systematic uncertainties which propagate from uncertain ratios between the peak and wing fluxes, including their color dependence in broad bands.

One way to decrease the exposure time and the degree of saturation is through spatial scanning during integration. Spatial scanning of the telescope reduces the effective exposure time a pixel "sees" a source in proportion to the inverse of the scan speed. The highest scan speed available with *HST* (requiring gyroscope guiding) is $7\farcs8$ s^{-1} which, for a pixel size of $0\farcs13$ for WFC3-IR, is 0.017 s, or 0.03 s including flux from the off-peak integration. At this speed saturation begins at $H = 7$ mag. This is just under half the minimum integration of the smallest subarray allowed. In the optical the advantage of scanning bright targets is even greater, where the $0\farcs04$ pixel of WFC3-UVIS and the PSF produce a minimum effective exposure time of 0.01 s, a factor of 50 shorter than the minimum allowed exposure, a saturation limit of $V = 7$ mag, and without uncertainties associated with a variable time of shutter flight. For increasingly brighter targets above the saturation limit, successive pairs of pixels adjacent to the peak saturate at a rate of approximately one new pixel pair per magnitude, and information is lost in blocks. For optical photometry with WFC3-UVIS, Gilliland et al. (2010) have shown that with a gain setting of 2 or higher, full-well saturation occurs before digital saturation, so that saturated star photometry is well measured by including the sum of the blooming charge in the total without loss in precision or accuracy.

Another advantage of scanning bright stars instead of taking pointed images with subarrays comes from improved sampling of the detector. Pixel-to- pixel variations in the flat fields or positional variation in quantum efficiency (QE) produces errors of about 0.01 mag with the WFC3-IR detector (Riess 2011). In addition, errors which depend on pixel phase (e.g., resulting from imperfect knowledge of the PSF) are reduced by scanning at an angle which varies the pixel phase, yielding a result that is independent of pixel phase.

3.2. SY Aurigae

On JD 2,455,989 we obtained scanned observations of the MW Cepheid SY Aur with WFC3-IR *F160W* at a commanded scan rate of $7\farcs5$/second.

We fit an empirical light profile (i.e., cross-section of a trailed PSF) to each minirow (i.e., a 21 pixel row centered on the source). The effective exposure time for each nondestructive sample of the HgCdTe detector is a fixed number (determined from ground-based testing, 0.853 s to read out the 512×512 pixel subarray utilized) plus an additional increment or decrement of exposure time to account for the altered position of the moving source relative to the detector. This additional

time is the standard interval between reads multiplied by the fractional increase or decrease of the array that must be read out before encountering the approaching or receding scan line (the sign of which depends on the scan direction and whether the scan is above or below the midline of the instrument which determines the readout direction).[7]

The difference in integration between an approaching and receding scan is quite large, amounting to an integration interval of 0.7092 s over a length of 44 pixels between samples when scanning toward the readout amplifier or 1.065 s over 65 pixels when scanning away from the readout. For each sample time interval, the count rate is measured from the product of the mean minirow count in the sample and the length of the sample scan divided by the time interval of the sample. The length divided by the interval is an empirical measure of the scan rate, which was found to be about 4% higher than requested. After rejecting the central pixel of each minirow which is slightly saturated, the measured count rate is 15.75 million e^- s^{-1} (*F160W* = 6.706 mag) scanning toward and 15.49 million e^- s^{-1} (*F160W* = 6.725 mag) scanning away. This 2% difference arises from edge effects causing us to overcount or undercount a partially filled pixel. We take the average of 6.716 ± 0.005 mag to cancel the edge effects. We increase this by 0.01 mag to 6.706 ± 0.005 mag to account for a 1% systematic underestimate of bright sources in short exposures where trapping is seen to reduce the measured charge by 1%. The row-to-row scatter is 3.25% and appears to result from nonsmooth scanning. It is worth noting that a fractional error in the WFC3-IR sample time, if uniform over all sample patterns (i.e., from the WFC3 clock running slow or fast), would be negated in the measurement of relative distances between MW and extragalactic Cepheids (when observed using the same clock).

Most known MW Cepheids have had their NIR light curves measured by Laney & Stoble (1992) or Monson & Pierce (2011). Their periods and phases have typically been determined to the third or fourth decimal place from optical light curves, which assures that photometry from a single epoch can be easily transformed to the mean magnitude with less than 1% statistical uncertainty (mean magnitudes are the standard measure used for Cepheid distance determinations as shown in Figure 8). For SY Aur, the expected difference between the single epoch and the mean in *F160W* is 0.05 mag, for a final result of $F160W = 6.67 \pm 0.01$ mag. With $E_{B-V} = 0.45$ mag and a period of 10.1 days, a Milky Way *P*–*L* relation (Benedict et al. 2007; Fouqué et al. 2007) would give a distance modulus of $\mu_0 = 11.96 \pm 0.12$ mag, in good agreement with the preliminary parallax distance modulus of $\mu_0 = 11.84$ mag measured here.

[7]A simplified analogy relates the exposure time to the time of flight for a ball traveling to a receiver who is moving toward or away from the ball.

4. Discussion

We have presented a new approach to measuring high precision, relative astrometry for stars with *HST* that can reach a final precision of 20–40 μas under optimal conditions. We obtained a preliminary measurement for the Cepheid SY Aurigae and several reference stars in its immediate neighborhood; this is the first of a planned 19 Galactic Cepheids to be measured with *HST* within the next two years.

Measuring accurate parallaxes while simultaneously characterizing this new observing mode has presented several new challenges. Examples include the impact of small variations in the telescope roll angle during observations, the small but significant differences in the geometric distortion solution as a function of filter and time, and the difficulties involved in matching observations across filters in order to tie the absolute parallax of the Cepheid target to that of a sufficient number of reference stars.

Some of these difficulties were unknown or not fully appreciated at the start of this two-year test program, the first of its kind, and have resulted in improvements in the selection of target fields and observing modes for subsequent targets. For example, doubling the number of shallow scans improves substantially the precision of the measurement, as shown in Figure 6. Other changes could not be applied effectively in the middle of the pilot campaign; for example, all targets selected for future observations have been chosen to have more bright reference stars, which yields an improved tie-in between target and reference stars, and the depth of the shallow scan has been more carefully optimized. These changes have improved the constraint on the Cepheid in the deep frame to 30–40 μas, as shown for two new fields in Figure 6.

For the remaining Cepheids, we have also acquired rapid boustrophedonic or "serpentine" scans with the broad filter to serve as an alternative to the narrow filter used for the shallow frame. This observing mode can in principle yield an additional improvement in the tie-in by a factor of the square root of the number of legs, typically 4 or 5, and from the homogeneity of filters used in transformations.

Lastly, we have found that we can improve on the polynomial characterization of the variable distortion; in practice, the 5- or even 9-parameter polynomial solutions appear to be restricted to a smaller set of effective parameters, which in principle can be identified and characterized through a principal-component analysis. We expect this type of analysis can be substantially improved with the availability of the statistics from the full program, including all Cepheids and calibration observations, in order to better understand and quantify the freedom required by the solution, and to improve our knowledge of the mapping between *HST's* thermal state and distortion.

The effort to measure parallaxes from space-based platforms for MW Cepheids has promise for anchoring a $\sim 1\%$ determination of the Hubble constant, an invaluable aid to cosmological investigations. Spatial scanning astrometry with *HST* may also be suitable for a much broader array of applications than considered here, including exoplanet detection from astrometric motion

or better relative astrometry improving constraints on microlensing events. Although the precision possible with this technique rivals that of GAIA and VLBI, the measurements are ultimately complementary because they can be collected for different types of objects (VLBI) or with a different class of systematics uncertainties (GAIA), to help ensure that parallax measurements of stars beyond a kiloparsec are robust.

This project was enabled by significant assistance from a wide variety of sources. We wish to thank Tom Harrison for his help determining the luminosity class of stars from their spectra. We thank Jeff Silverman, Kelsey Clubb, Brad Cenko, Brad Tucker, and Waqas Bhatti for their help obtaining and calibrating the spectra of reference stars in the field of SY Aur; the staff at Lick Observatory also assisted. Merle Reinhardt, George Chapman, William Januszewski, and Ken Sembach provided help with the *HST* observations. We thank Ed Nelan and Fritz Benedict for productive discussions about the behavior of the FGS. We also thank Leo Girardi, Alessandro Bressan, Paola Marigo, for the use of and assistance with their Padova isochrone database. Support for this work was provided by NASA through programs GO-12679 and GO-13101 from the Space Telescope Science Institute, which is operated by AURA, Inc., under NASA contract NAS 5-26555. A.V.F. is grateful for financial support from NSF grant AST-1211916, the TABASGO Foundation, and the Christopher R. Redlich Fund.

REFERENCES

Bellini, A., Anderson, J., & Bedin, L. R. 2011, PASP, 123, 622

Benedict, G. F., McArthur, B. E., Feast, M. W., Barnes, T. G., Harrison, T. E., Patterson, R. J., Menzies, J. W., Bean, J. L., & Freedman, W. L. 2007, AJ, 133, 1810

Bressan, A., Marigo, P., Girardi, L., Salasnich, B., Dal Cero, C., Rubele, S., & Nanni, A. 2012, MNRAS, 427, 127

Duquennoy, A. & Mayor, M. 1991, A&A, 248, 485

Fouqué, P., Arriagada, P., Storm, J., Barnes, T. G., Nardetto, N., Mérand, A., Kervella, P., Gieren, W., Bersier, D., Benedict, G. F., & McArthur, B. E. 2007, A&A, 476, 73

Freedman, W. L., Madore, B. F., Gibson, B. K., Ferrarese, L., Kelson, D. D., Sakai, S., Mould, J. R., Kennicutt, Jr., R. C., Ford, H. C., Graham, J. A., Huchra, J. P., Hughes, S. M. G., Illingworth, G. D., Macri, L. M., & Stetson, P. B. 2001, ApJ, 553, 47

Freedman, W. L., Madore, B. F., Scowcroft, V., Burns, C., Monson, A., Persson, S. E., Seibert, M., & Rigby, J. 2012, ApJ, 758, 24

Gilliland, R. L., Rajan, A., & Deustua, S. 2010, WFC3 UVIS Full Well Depths, and Linearity Near and Beyond Saturation, Tech. rep.

Hu, W. 2005, Phys. Rev. D, 71, 047301

Humphreys, E. M. L., Reid, M. J., Moran, J. M., Greenhill, L. J., & Argon, A. L. 2013, ApJ, 775, 13

Kalirai, J. S., Deustua, S., Rajan, A., & Riess, A. 2011, The Photometric Performance of WFC3/IR: Temporal Stability Through Year 1, Tech. rep.

Laney, C. D. & Stoble, R. S. 1992, A&AS, 93, 93

Leavitt, H. S. & Pickering, E. C. 1912, Harvard College Observatory Circular, 173, 1

McCullough, P. & MacKenty, J. 2012, Considerations for using Spatial Scans with WFC3, Tech. rep.

Monson, A. J. & Pierce, M. J. 2011, ApJS, 193, 12

Nelan, E. 2012, Fine Guidance Sensor Instrument Handbook for Cycle 21 v.20.0

Ngeow, C.-C., Kanbur, S. M., Nikolaev, S., Buonaccorsi, J., Cook, K. H., & Welch, D. L. 2005, MNRAS, 363, 831

Perryman, M. 2009, Astronomical Applications of Astrometry: Ten Years of Exploitation of the Hipparcos Satellite Data (Cambridge University Press)

Pickles, A. J. 1998, PASP, 110, 863

Prugniel, P. & Soubiran, C. 2001, VizieR Online Data Catalog, 3218, 0

Reid, M. J. & Honma, M. 2013, ArXiv e-prints

Riess, A. G. 2011, An Independent Determination of WFC3-IR Zeropoints and Count Rate Non-Linearity from 2MASS Asterisms, Tech. rep.

Riess, A. G., Macri, L., Casertano, S., Lampeitl, H., Ferguson, H. C., Filippenko, A. V., Jha, S. W., Li, W., & Chornock, R. 2011, ApJ, 730, 119

Riess, A. G., Macri, L., Li, W., Lampeitl, H., Casertano, S., Ferguson, H. C., Filippenko, A. V., Jha, S. W., Chornock, R., Greenhill, L., Mutchler, M., Ganeshalingham, M., & Hicken, M. 2009, ApJS, 183, 109

Robin, A. & Crézé, M. 1986, A&A, 157, 71

Robin, A. C., Reylé, C., Derrière, S., & Picaud, S. 2003, A&A, 409, 523

Sandage, A., Tammann, G. A., Saha, A., Reindl, B., Macchetto, F. D., & Panagia, N. 2006, ApJ, 653, 843

Schlegel, D. J., Finkbeiner, D. P., & Davis, M. 1998, ApJ, 500, 525

Skrutskie, M. F., Cutri, R. M., Stiening, R., Weinberg, M. D., Schneider, S., Carpenter, J. M., Beichman, C., Capps, R., Chester, T., Elias, J., Huchra, J., Liebert, J., Lonsdale, C., Monet, D. G., Price, S., Seitzer, P., Jarrett, T., Kirkpatrick, J. D., Gizis, J. E., Howard, E., Evans, T., Fowler, J., Fullmer, L., Hurt, R., Light, R., Kopan, E. L., Marsh, K. A., McCallon, H. L., Tam, R., Van Dyk, S., & Wheelock, S. 2006, AJ, 131, 1163

Sorce, J. G., Tully, R. B., & Courtois, H. M. 2012, ApJ, 758, L12

Sullivan, M., Guy, J., Conley, A., Regnault, N., Astier, P., Balland, C., Basa, S., Carlberg, R. G., Fouchez, D., Hardin, D., Hook, I. M., Howell, D. A., Pain, R., Palanque-Delabrouille, N., Perrett, K. M., Pritchet, C. J., Rich, J., Ruhlmann-Kleider, V., Balam, D., Baumont, S., Ellis, R. S., Fabbro, S., Fakhouri, H. K., Fourmanoit, N., González-Gaitán, S., Graham, M. L., Hudson, M. J., Hsiao, E., Kronborg, T., Lidman, C., Mourao, A. M., Neill, J. D., Perlmutter, S., Ripoche, P., Suzuki, N., & Walker, E. S. 2011, ApJ, 737, 102

Suyu, S. H., Hensel, S. W., McKean, J. P., Fassnacht, C. D., Treu, T., Halkola, A., Norbury, M., Jackson, N., Schneider, P., Thompson, D., Auger, M. W., Koopmans, L. V. E., & Matthews, K. 2012a, ApJ, 750, 10

Suyu, S. H., Treu, T., Blandford, R. D., Freedman, W. L., Hilbert, S., Blake, C., Braatz, J., Courbin, F., Dunkley, J., Greenhill, L., Humphreys, E., Jha, S., Kirshner, R., Lo, K. Y., Macri, L., Madore, B. F., Marshall, P. J., Meylan, G., Mould, J., Reid, B., Reid, M., Riess, A., Schlegel, D., Scowcroft, V., & Verde, L. 2012b, ArXiv e-prints

Tammann, G. A., Sandage, A., & Reindl, B. 2003, A&A, 404, 423

van Altena, W. F., Lee, J. T., & Hoffleit, E. D. 1995, The general catalogue of trigonometric [stellar] parallaxes

Weinberg, D. H., Mortonson, M. J., Eisenstein, D. J., Hirata, C., Riess, A. G., & Rozo, E. 2013, Phys. Rep., 530, 87

This preprint was prepared with the AAS LaTeX macros v5.2.

Table 1. Spatial scanning observations used in this paper

Date	Rootname	Program ID	EXPSTART (MJD)	Filter	Exp. time (seconds)	Scan rate (″/second)	Scan length (″)
SY Aurigae							
2011-09-26	ibtq21gfq	12679	55830.87723571	*F606W*	455	0.316	143.78
2011-09-26	ibtq21ghq	12679	55830.88444645	*F673N*	348	0.414	144.07
2011-09-26	ibtq21gfq	12679	55830.87723571	*F606W*	455	0.316	143.78
2012-03-02	ibx202j3q	12794	55988.55573488	*F606W*	405	0.355	143.77
2012-03-02	ibx202j7q	12794	55988.56899858	*F606W*	405	0.355	143.77
2012-03-02	ibx202jbq	12794	55988.58226266	*F606W*	405	0.355	143.77
2012-03-02	ibtq24jkq	12679	55988.62925340	*F606W*	455	0.316	143.78
2012-03-02	ibtq24jmq	12679	55988.63651007	*F673N*	348	0.414	144.07
2012-09-16	ibtq25qcq	12679	56186.80378314	*F673N*	380	0.379	144.02
2012-09-16	ibtq25qeq	12679	56186.80970907	*F673N*	380	0.379	144.02
2012-09-16	ibtq25qaq	12679	56186.79652610	*F606W*	455	0.316	143.78
2012-09-16	ibtq25qgq	12679	56186.81616721	*F606W*	455	0.316	143.78
2013-03-03	ibtq26odq	12679	56354.53130985	*F673N*	380	0.379	144.02
2013-03-03	ibtq26ofq	12679	56354.53723577	*F673N*	380	0.379	144.02
2013-03-03	ibtq26obq	12679	56354.52405281	*F606W*	455	0.316	143.78
2013-03-03	ibtq26ohq	12679	56354.54369429	*F606W*	455	0.316	143.78
2013-08-25	ic4010ncq	13101	56529.04306131	*F606W*	348	0.410	142.68
2013-08-25	ic4010neq	13101	56529.04884834	*F673N*	348	0.410	142.68
M35							
2012-12-16	ic4001vjq	13101	56277.55560208	*F606W*	350	0.410	143.50
2012-12-16	ic4001vlq	13101	56277.56118097	*F606W*	350	0.410	143.50
2012-12-16	ic4001vnq	13101	56277.56675949	*F606W*	350	0.410	143.50
2012-12-16	ic4001vpq	13101	56277.57233837	*F606W*	350	0.410	143.50
2012-12-16	ic4001vrq	13101	56277.57791689	*F606W*	350	0.410	143.50
2012-12-16	ic40a1vwq	13101	56277.62121541	*F606W*	350	0.410	143.50
2012-12-16	ic40a1vyq	13101	56277.62679430	*F606W*	350	0.410	143.50
2012-12-16	ic40a1w0q	13101	56277.63237282	*F606W*	350	0.410	143.50
2012-12-16	ic40a1w2q	13101	56277.63795171	*F606W*	350	0.410	143.50
2012-12-16	ic40a1w4q	13101	56277.64353023	*F606W*	350	0.410	143.50
2012-12-17	ic4003bjq	13101	56278.22042837	*F621M*	350	0.410	143.50
2012-12-17	ic4003blq	13101	56278.22600726	*F621M*	350	0.410	143.50
2012-12-17	ic4003bnq	13101	56278.23158578	*F621M*	350	0.410	143.50
2012-12-17	ic4003brq	13101	56278.23716467	*F621M*	350	0.410	143.50
2012-12-17	ic4003btq	13101	56278.24274319	*F621M*	350	0.410	143.50
2012-12-17	ic40a3c5q	13101	56278.28586837	*F673N*	350	0.410	143.50
2012-12-17	ic40a3c7q	13101	56278.29144689	*F673N*	350	0.410	143.50
2012-12-17	ic40a3c9q	13101	56278.29702578	*F673N*	350	0.410	143.50
2012-12-17	ic40a3cbq	13101	56278.30260430	*F673N*	350	0.410	143.50
2012-12-17	ic40a3cdq	13101	56278.30818319	*F673N*	350	0.410	143.50

Table 1—Continued

Date	Rootname	Program ID	EXPSTART (MJD)	Filter	Exp. time (seconds)	Scan rate (″/second)	Scan length (″)
2012-12-24	ic4002aiq	13101	56285.66540541	*F606W*	350	0.410	143.50
2012-12-24	ic4002akq	13101	56285.67098393	*F606W*	350	0.410	143.50
2012-12-24	ic4002amq	13101	56285.67656282	*F606W*	350	0.410	143.50
2012-12-24	ic4002aoq	13101	56285.68214134	*F606W*	350	0.410	143.50
2012-12-24	ic4002aqq	13101	56285.68772023	*F606W*	350	0.410	143.50
2012-12-24	ic40a2avq	13101	56285.73057912	*F606W*	350	0.410	143.50
2012-12-24	ic40a2axq	13101	56285.73615763	*F606W*	350	0.410	143.50
2012-12-24	ic40a2azq	13101	56285.74173652	*F606W*	350	0.410	143.50
2012-12-24	ic40a2b1q	13101	56285.74731504	*F606W*	350	0.410	143.50
2012-12-24	ic40a2b3q	13101	56285.75289356	*F606W*	350	0.410	143.50
2013-01-03	ic4004dpq	13101	56295.50244302	*F621M*	350	0.410	143.50
2013-01-03	ic4004drq	13101	56295.50802154	*F621M*	350	0.410	143.50
2013-01-03	ic4004dtq	13101	56295.51360043	*F621M*	350	0.410	143.50
2013-01-03	ic4004dvq	13101	56295.51917895	*F621M*	350	0.410	143.50
2013-01-03	ic4004dxq	13101	56295.52475783	*F621M*	350	0.410	143.50
2013-01-03	ic40a4e2q	13101	56295.56700302	*F673N*	350	0.410	143.50
2013-01-03	ic40a4e4q	13101	56295.57258191	*F673N*	350	0.410	143.50
2013-01-03	ic40a4e6q	13101	56295.57816043	*F673N*	350	0.410	143.50
2013-01-03	ic40a4e8q	13101	56295.58373932	*F673N*	350	0.410	143.50
2013-01-03	ic40a4eaq	13101	56295.58931783	*F673N*	350	0.410	143.50

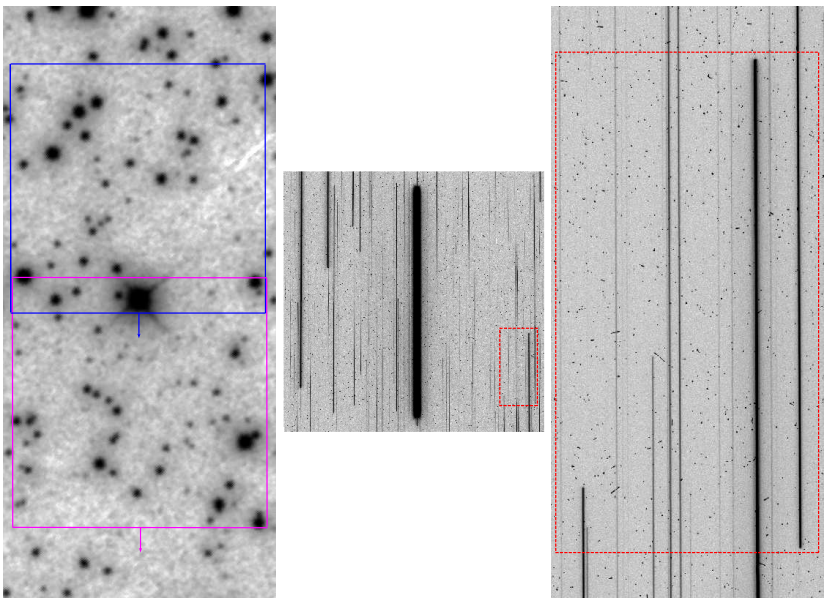

Fig. 1.— (Left) Digital Sky Survey image of the field centered around Cepheid SY Aur covered by WFC3-UVIS spatial scanning. (Middle) Scan image of the field in *F606W* from DD program 12879. Points become parallel lines with a greatly increased number of samples along the scan direction and relative astrometry precision *perpendicular* to the scan. (Right) Scan field marked with a box in the middle panel, magnified by a factor of 7.

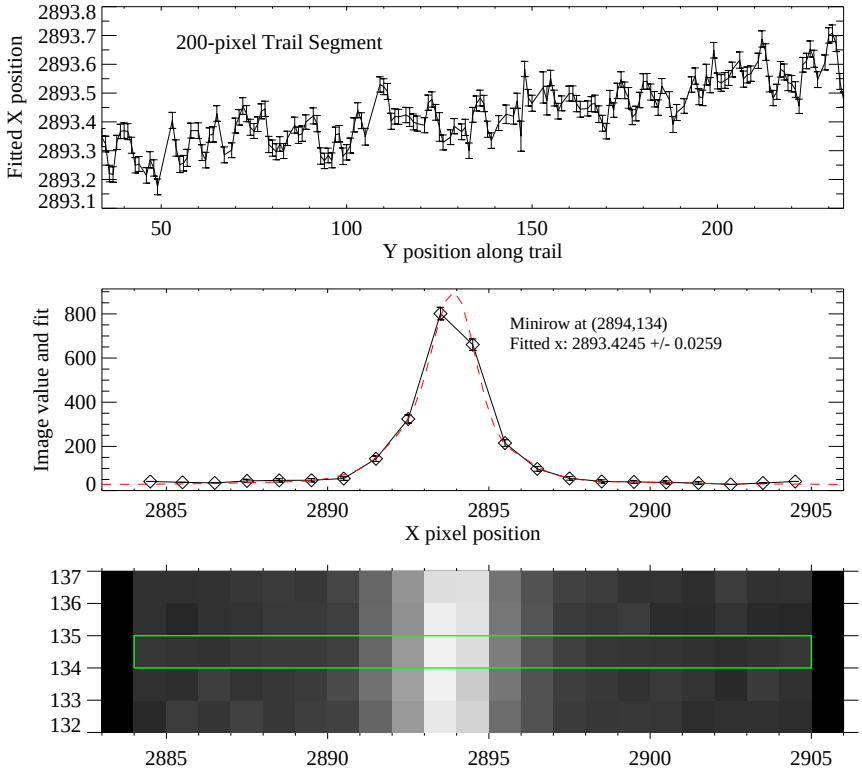

Fig. 2.— The "minirow" unit of measure for spatial scans. 21-pixel rows centered on each scan line and their pixel values and data quality flags (bottom) are used to measure the star position along the row by fitting a section of a PSF (middle). Measurement of line positions in the detector x-coordinate reveal telescope jitter (top).

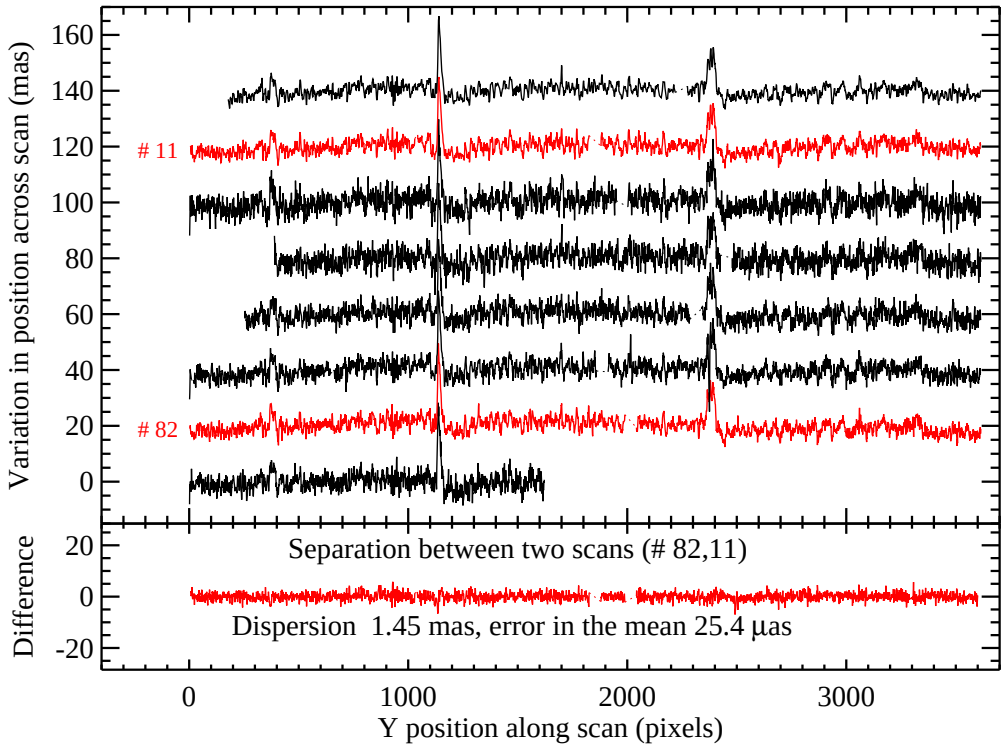

Fig. 3.— (Top) Measured position of selected stars in the scanned image of SY Aur, after subtraction of a low-order polynomial. Correlated offsets indicate telescope jitter perpendicular to the scan. (Bottom) Difference in position perpendicular to the scan, the direction of parallax, for two stars. The difference removes the jitter noise which is correlated for each star and averages down to a mean 25 μas precision.

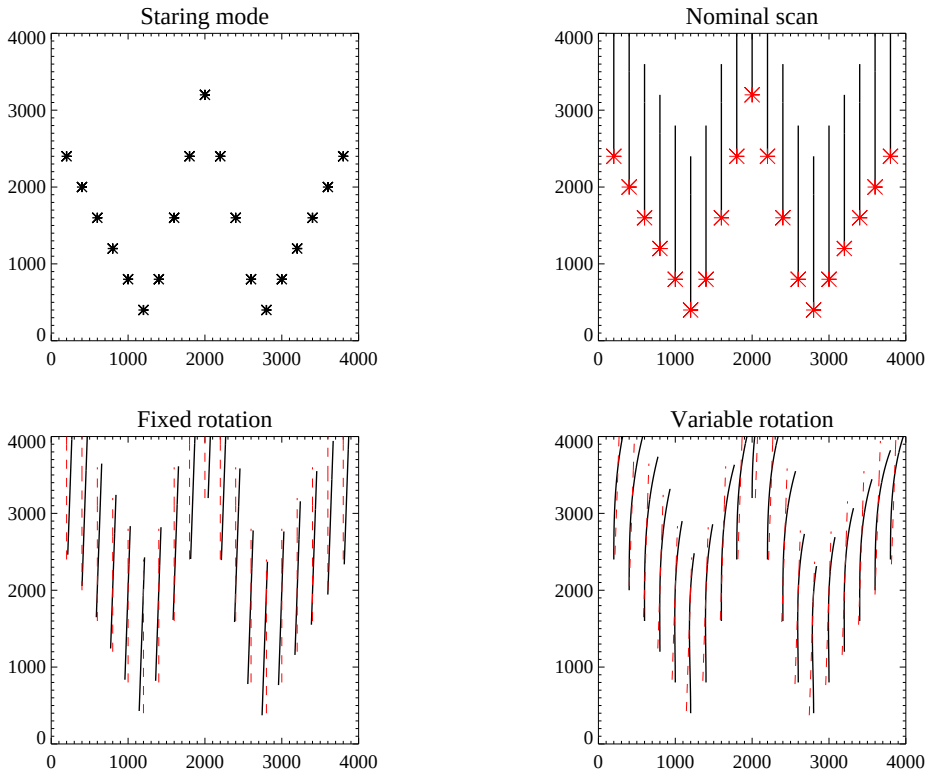

Fig. 4.— Illustrations of the effect of static or variable rotation of the telescope on lines during spatial scanning. Fixed rotation and variable rotation, the latter causing nonparallelism of scan lines, must be measured and corrected from the rectified scan lines.

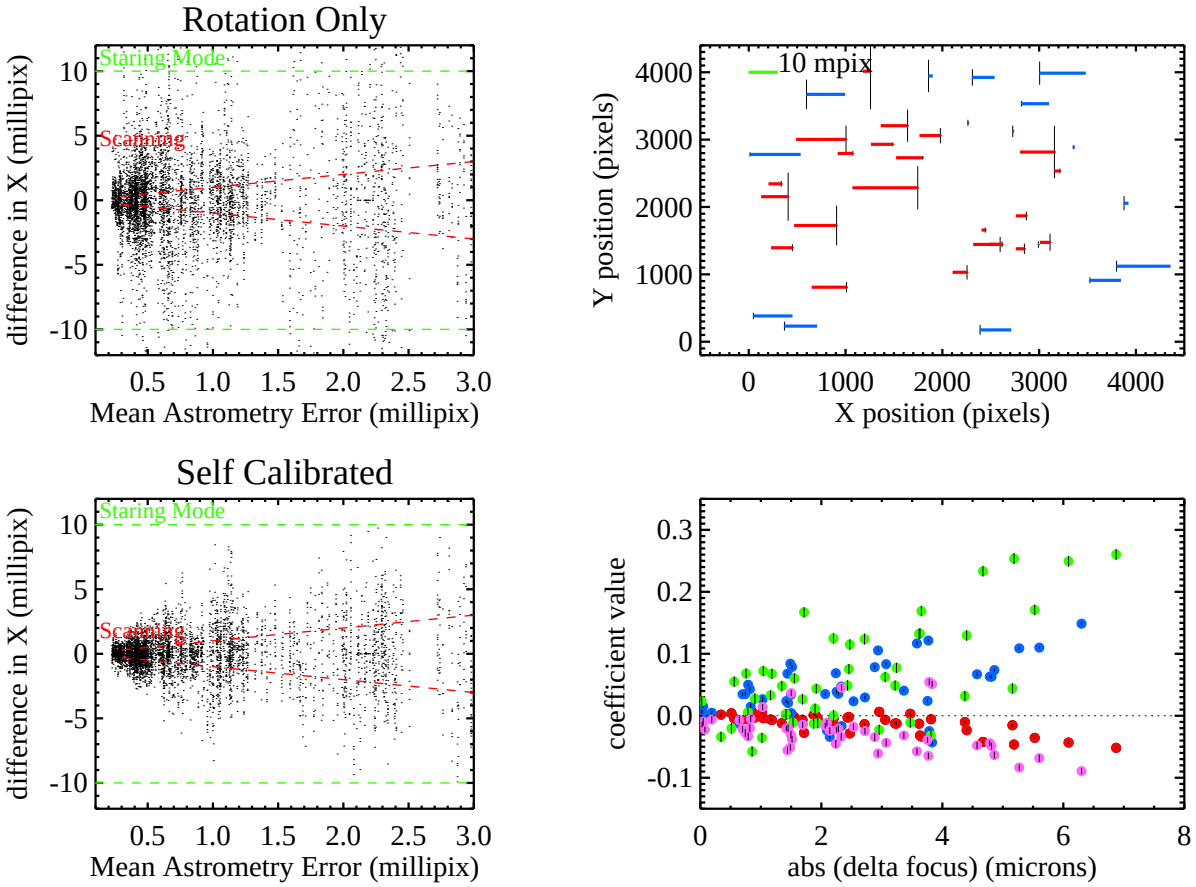

Fig. 5.— Calibration of frame-to-frame variable distortion from observations of stars in M35. Excess dispersion in the relative positions of stars over a continuous sequence of scans is apparent (upper left). Relating the position differences to the mean location of each star on the detector reveals large-scale distortions. A low-order polynomial can be used to measure and remove these time-dependent distortions (lower left) to reach (or nearly reach) the photon statistics. The polynomial coefficients appear to correlate with the modeled thermal state of *HST* and the modeled focus position resulting from thermally induced piston motion of the secondary.

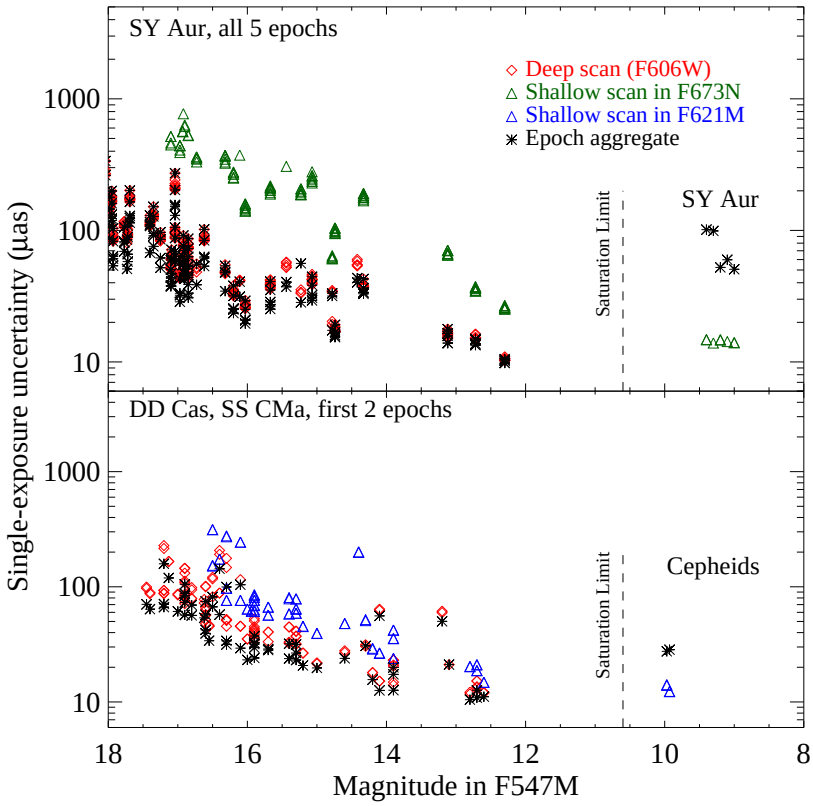

Fig. 6.— Astrometric precision of star positions in spatial scans of Cepheid fields. A deep scan in *F606W* (shown in red) measures many stars to better than 40 μas but saturates the Cepheid. A shallow scan in *F673N* (green) measures the Cepheid to $\sim 20\,\mu$as, but the paucity of stars with measurements better than 100 μas reduces the precision of the modeled position of SY Aur in the deep frame. By choosing a field with more reference stars, using a more efficient filter, and doubling the number of scans, we can measure Cepheids to $\sim 30\,\mu$as (bottom panel).

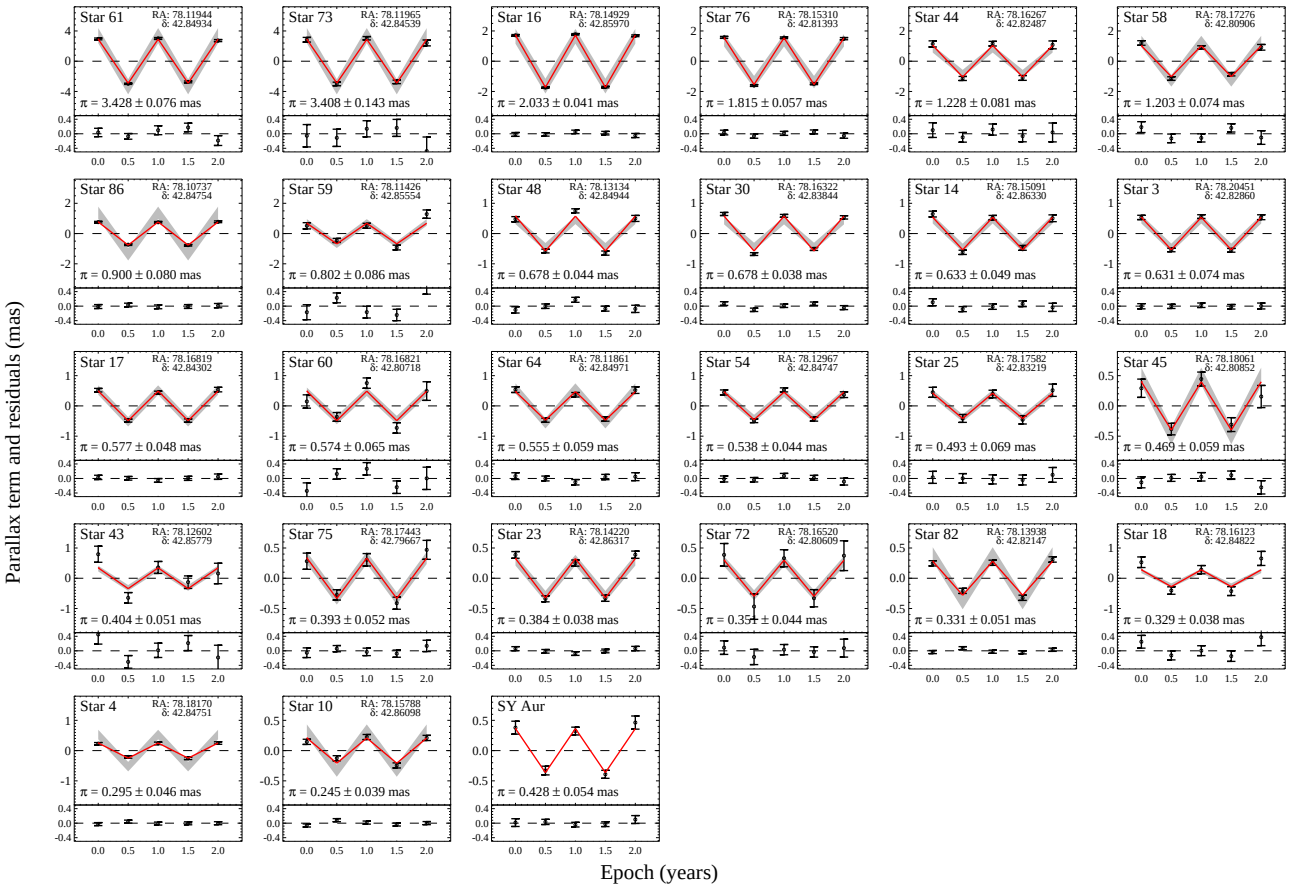

Fig. 7.— Individual stellar parallaxes in the field of SY Aur. Ordered from closest to farthest are the measured parallax (red line) and spectrophotometric parallax (grey band with $\pm 2\sigma$ width) used to reduce parallaxes from relative to absolute. Fitted proper motions have been subtracted from the measurements and fits for ease of viewing. Stars 4 and 10 are red giants with parallaxes yielding $D = 3.4 \pm 0.5$ and 4.1 ± 0.6 kpc. The Cepheid SY Aur has a parallax yielding $D = 2.3$ kpc, in good agreement with an expectation of 2.1 kpc from the P–L relation.

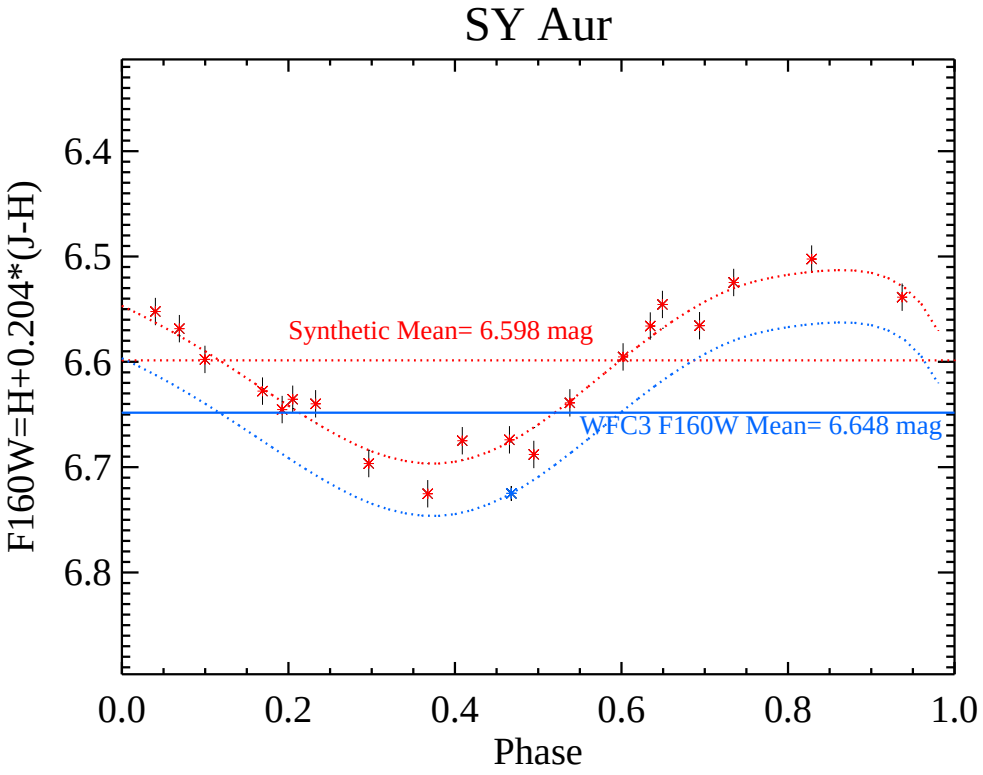

Fig. 8.— Near-infrared spatial scan photometry of SY Aur. A photometric measurement with WFC3-UVIS *F160W* is transformed from the indicated phase to the mean using the J and H-band light curves from Monson & Pierce (2011). The result is a measurement on the same photometric system routinely used for extragalactic Cepheids at $D > 20\,\mathrm{Mpc}$.